Microchimica Acta (2021) 188:75
https://doi.org/10.1007/s00604-021-04721-4

ORIGINAL PAPER

Liposome encapsulated electron donor strategy for signal-on CYFRA 21-1 photoelectrochemical analysis

Rui Xu[1] · Yu Du[1] · Lei Liu[1] · Dawei Fan[1] · Xiang Ren[1] · Xuejing Liu[1] · Qin Wei[1] · Huangxian Ju[1,2]

Received: 3 December 2020 / Accepted: 19 January 2021

Abstract

A novel electron donor controlled-release system is proposed based on liposome encapsulated L-cysteine for the sensitive determination of cytokeratin 19 fragment 21–1 (CYFRA 21-1). On the one hand, a defective TiO_2 modified with methylene blue was employed as a photoactive platform which exhibited a high photoelectrochemical (PEC) response owing to the introduction of oxygen vacancies and the high photosensitivity of the dye. On the other hand, L-cysteine as the sacrificial electron donor was encapsulated in the vesicles of liposomes, and this composite was used as the signal amplification factor, which is labeled on the secondary antibody of CYFRA 21-1 to further improve the photocurrent sensitivity. The excellent electron transfer path in photoactive materials coupled with the skilful electron donor controlled-release system, contributed to the sensitive PEC analysis of CYFRA 21-1 underoptimum conditions. The PEC immunoassay showed a linear current response in the range 0.0001–100 ng/mL with a detection limitof 37 fg/mL. Enhanced stability and satisfactory reproducibility were also achieved. The proposed concept provides a novel signal-on strategy for the sensitive detection of other cancer markers in the electrochemical sensing field.

Keywords Liposome · L-cysteine · Defective TiO_2 · Methylene blue · CYFRA 21-1

Introduction

Cancer has become the number one killer of humans, and the morbidity and mortality of the lung cancer are the highest in the world [1, 2]. The early detection and treatment of lung cancer can effectively suppress the rise in mortality. Cytokeratin 19 fragment antigen 21–1 (CYFRA 21-1), as a soluble fragment, is a new lung cancer marker, which is currently being studied very actively, especially for non-small cell lung cancer [3, 4]. Thus, lung cancer can be quickly analyzed to a certain degree by the sensitive and accurate detection of CYFRA 21-1 in serum. Previously, researchers made many attempts to detect CYFRA 21-1 via some methods, including enzyme-linked immunosorbent assay [5], electrochemiluminescence [6], electrochemical [7], and chemiluminescence [8]. Among these methods, the photoelectrochemical (PEC) assay, which exhibits ultrasensitive detection characteristics due to the special way of signal conversion [9–11], was employed in this work for CYFRA 21-1 detection.

For PEC analyses, photosensitive materials are the foundation for sensing platform construction. As one of the metal oxide semiconductor materials, titanium dioxide is widely used in photocatalysis and photoelectric analyses owing to its excellent photosensitive property [12–14], but the wide band gap (~3.2 eV) hinders the visible light usage efficiency. Defect engineering is diffusely approved, and it is considered to be an effective method to advance the PEC activity. Including oxygen vacancies [15] is one of the useful method of introducing defects to TiO_2 , providing surface active sites to promote photocatalytic activation [16], and narrowing its band gap [17]. Among them, oxygen vacancy as the most prevalent defect was employed in this work to perfect

✉ Xuejing Liu
chm_liuxj@ujn.edu.cn

✉ Qin Wei
sdjndxwq@163.com

[1] Collaborative Innovation Center for Green Chemical Manufacturing and Accurate Detection, Key Laboratory of Interfacial Reaction & Sensing Analysis in Universities of Shandong, University of Jinan, Jinan 250022, Shandong, China

[2] State Key Laboratory of Analytical Chemistry for Life Science, School of Chemistry and Chemical Engineering, Nanjing University, Nanjing 210023, China

Published online: 09 February 2021

the photoactivity of TiO_2 [18–20]. The formation of oxygen vacancies in the crystal lattice usually adopts doped metals or non-metal ions. For example, Wu and co-workers reported the replacement of Cu^{2+} for Ti^{4+} ions in the lattice which can realize the generation of oxygen vacancies in the lattice of TiO_2 [21]. In this work, the trivalent cation Fe^{3+} was used to dope in the lattice of TiO_2 and occupy the Ti^{4+} sites. While doping of Fe^{3+}, oxygen vacancies were introduced, which greatly improved the utilization efficiency of the visible light, and accelerated the generation of photo-generated electrons. For another, a shallow defect energy level just below the conduction band of TiO_2 was introduced via the Fe^{3+} doping, which also contributed to the visible light response [15]. Furthermore, considering the outstanding photoelectric conversion ability of dyes [22–25], methylene blue (MB), which has prominent charge transfer properties was used to sensitize defective TiO_{2-x} to further improve the stability of PEC platform, and it is also one of the most promising pathways for improving the sensitivity of PEC biosensors.

In addition to modifying the photoactive material to perfect the PEC response, adding electron donor into the detection electrolyte solution can also increase the photocurrent and improve the sensitivity of the sensor. Different from adding excessive electron donor directly to the detection solution, the electron donor controlled-release system can effectively improve the sensitivity of the biosensor for target detection [26–28]. Liposome is a microscopic spherical vesicle with hollow cavities, and the specific molecules or nanomaterials can be trapped in their cavities or anchored on their surfaces to deliver various species [29, 30]. In this work, L-cysteine (electron donor), which is a common amino acid, was encapsulated in the liposome thanks to the great biocompatibility, and the complex act as a marker labeled on the secondary antibody (Ab_2). The liposome could be dissolved by tween and easily released from the vesicae of the liposome. Thus, the L-cysteine can be released to increase photocurrent. The amount of electron donor released increases with the increased concentration of target antigen, therefore achieving the sensitive CYFRA 21-1 detection. Compared with other electrochemical methods, this novel controlled-release system greatly improved the detection range and reduced the detection limits.

Experimental section

Preparation of liposome@L-cysteine-Ab_2 bioconjugate

The preparation of liposome@L-cysteine was produced via a simple method. Briefly, 0.02 g of 1,2-dipalmitoyl-sn-glycero-3-phosphocholine, 0.015 g of cholesterol, and 0.005 g of 1,2-dipalmitoyl-sn-glycero-3-phosphoethanolamine were co-dispersed into 5 mL of chloroform, and the mixture was bubbled with nitrogen and ultrasonic for 10 min, after which the solvent was removed via vacuum rotary evaporation. Thereafter, the product was added to an L-cysteine solution (5 mL, 25 mM) and allowed to incubated at 45 °C for 2 h. Finally, the redundant L-cysteine was eliminated by dialyzing against ultrapure water for 24 h under natural environment. The obtained liposome@L-cysteine was stored at 4 °C for future use.

The liposome@L-cysteine-Ab_2 bioconjugate was prepared as follows: 20 μL of EDC (5 mg/mL) and 20 μL of NHS (1 mg/mL) were added in 1 mL of the as-prepared liposome@L-cysteine solution. The mixture was shaken for 15 min under room atmosphere. After that, 1 mL of Ab_2 (10 μg/mL) was injected, and the bio-mixture was incubated at 30 °C for 5 h. After the incubation. Then, the bioconjugate was centrifuged at 4500 r and then dispersed in 2 mL of PBS buffer solution (pH 7.4) and stored at 4 °C for later use. Further details of the material preparation process details are present in the *Electronic Supplementary Material* (ESM) file.

The assembly of PEC biosensor

The assembly procedure of the proposed PEC biosensor is shown in Fig. 1. Indium tin oxide (ITO) conductive glass electrodes as the basic support for biosensor fabrication were ultrasonic prewashed with liquid detergent, acetone, ethanol, and ultrapure water. First, 10 μL of defective TiO_{2-x} (3 mg/mL) was modified on the cleaning ITO electrode, and then calcined at 450 °C for 1 h. After that, 6 μL of MB-Ab_1 solution was modified on the photosensitive platform and allow incubated for 40 min (MB was difficult to combined with defective TiO_{2-x} [31], incubating it with the Ab_1 via cross-linking agent to form the complex, which could reduce the fabrication steps). After washed the electrodes with PBS buffer solution, 4 μL of BSA (1w%) was decorated on the photoanode and washed after 40 min. Subsequently, 6 μL of various concentrations of Ag was modified and incubated for 40 min. Finally, the washed electrodes were modified with 6 μL of liposome@L-Cysteine-Ab_2 bioconjugate, due to the specific reaction between antigen and antibody and the concentration of Ag determined the modification concentration of liposome@L-cysteine; thus, the different PEC responses were obtained for the target detection.

Real sample treatment and PEC measurement

In order to characterize the detection accuracy of the PEC biosensor, a standard addition method was used to analyze the real sample detection. Prior to measurement, the serum samples were centrifuged at 2800 rpm under 4 °C for 10 min to receive the supernatants, which were used as the detection samples. When the levels of serum CYFRA 21-1 were found to be outside the calibration range, the serum

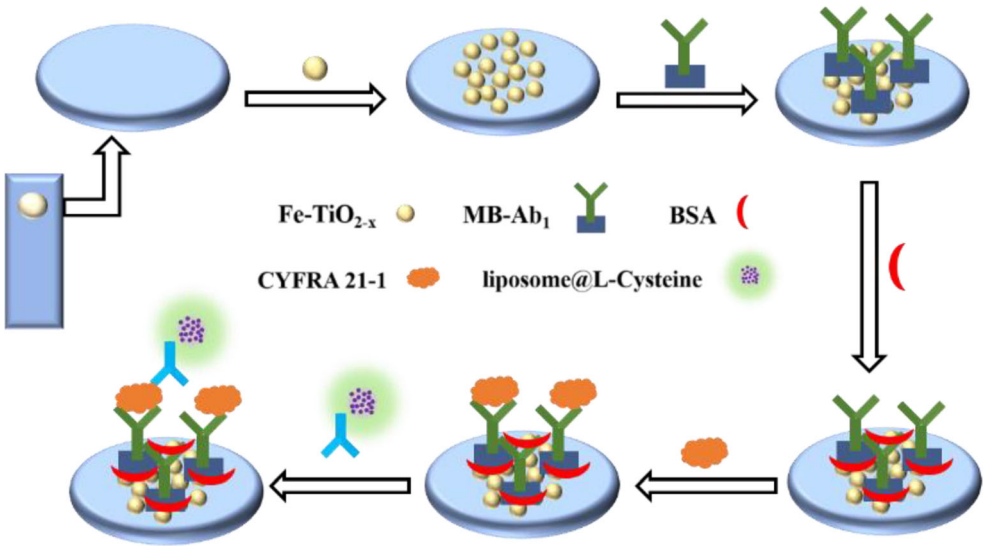

Fig. 1 The fabrication process of the PEC biosensor

sample was diluted with PBS (0.1 M, pH 7.4) and acquired two practical samples which with the concentrations were 0.58 ng/mL and 4.73 ng/mL. The PEC measurement was done in a photosensitive cell containing 10 mL PBS buffer (pH 7.4) solution with or without tween (20 μL). The prepared electrode as the work electrode with platinum electrode (counter electrode) and saturated calomel electrode (SCE) (reference electrode) constituted the three-electrode system of electrochemical workstation. The LED lamp (white light) was used as the excitation source, and it is switched every 10 s under 0 V voltage (vs. SCE) to test the photocurrent.

Results and discussion

Characterization of materials

As the basis of sensor construction, photosensitive materials are characterized before the PEC analysis platform fabrication Firstly, the material was characterized by X-ray powder diffraction (XRD) to determine if it was successfully synthesized. As shown in Fig. 2a, the peaks of the prepared pure TiO_2 fitted perfectly with the standard card (JCPDS No. 21–1272). The sharp peaks of Fe-TiO_{2-x} also match well with the standard card, and the peak of (101) crystal planes was stronger than that of the pure TiO_2. Figure 2b shows the sheet-like morphology of TiO_{2-x}, which could be offer convenient for visible-light absorption and fix other photosensitive materials because of the large surface area. Also, the excellent structure may offer a suitable electron transfer path to enhance the PEC response. Figure 2c shows the ultraviolet-visible absorption spectrum of the solid-state TiO_2 and Fe-TiO_{2-x}. Fe-TiO_{2-x} had a wider absorption range than TiO_2 and a strong absorption peak at about 580 nm, which is consistent with the luminous intensity of the employed light source (Fig. S1), proving that the prepared defective TiO_{2-x} has stronger light absorption performance. The X-ray photoelectron spectroscopy (XPS) image (Fig. 2d) shows that the Fe element was successfully doped into TiO_{2-x}. The Ti 2p spectrum has two fitting peaks, the peak at 458.1 eV corresponding to Ti $2p_{3/2}$ and the peak at 463.8 eV corresponding to Ti $2p_{1/2}$. These two peaks represent the Ti^{4+}state of TiO_{2-x} (Fig. 2e). The O 1 s spectra (Fig. 2f) have fitted peaks at 529.6 eV and 530.6 eV, which were attributed to the lattice oxygen and oxygen defects of TiO_{2-x}, respectively. The peak at 529.4 eV is attributed to the blue-shift of the oxygen absorption, and it implies that the surface oxygen-related defects were enhanced [21]. Figure S2 shows the energy dispersive X-ray spectroscopy (EDS) image of the Fe-TiO_{2-x}, which further conforms the successful doping of Fe, and the content ratio of each element is shown in Table S1 (ESM file).

Mechanism study of the PEC platform

The possible principle of electron transfer in the proposed PEC platform was explored and is shown in Fig. 3. Through the doping of Fe^{3+}, the defective TiO_{2-x} contains more oxygen vacancies, which could accelerate the transmission of electrons. Besides, via Fe doping, the band gap of TiO_2 would be narrowed, and the allowable light excitation path increases with the generation of impurity energy levels, which would cause a significant red shift in its UV absorption spectrum and increase the utilization of the visible light. After decorating with MB, the photo-induced electrons on the excited dye transferred into the defective TiO_{2-x}, and the PEC response was further increased; hence, the stability of the photoactive platform was improved. At the same time, L-cysteine as an electron donor was encapsulated in the liposome vesicles, and as the signal enhancer labeled on Ab_2, when the fabricated PEC biosensor was dipped in PBS solution containing tween,

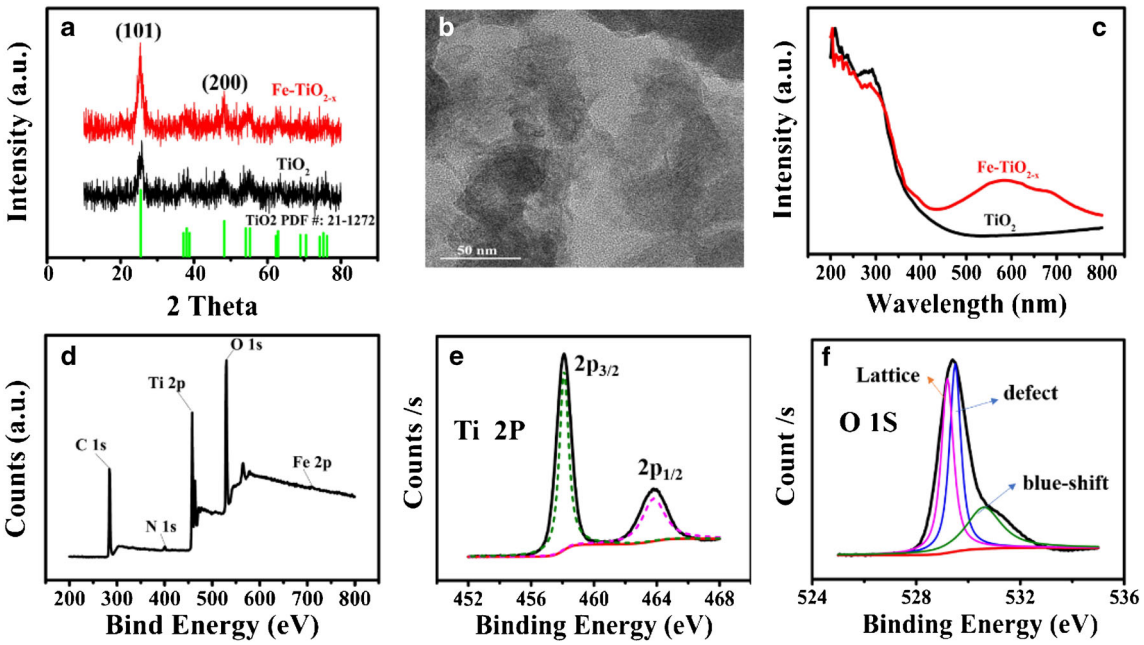

Fig. 2 **a** The XRD image of TiO_2 and Fe-TiO_{2-x}, **b** the TEM image of Fe-TiO_{2-x}, **c** the UV–vis diffuse reflectance spectra of TiO_2 and Fe-TiO_{2-x}, **d** the XPS image of Fe-TiO_{2-x}, and the XPS image of the element of **e** Ti 2p and **f** O 1 s

the liposome dissolved and the L-cysteine released to react with the photo-generated holes, following the PEC response increased. Thus, various target concentrations were detected at different signal amplification, a super sensitivity PEC biosensor was realized by this skillful strategy.

Sensor performance characterization

Herein, the skillful PEC biosensor was constructed via a layer-by-layer process for target detection, and it is necessary to determine if the layer-by-layer modification processes were successful. Testing the PEC signal after modifying each layer on the ITO electrode is a common and effective way to determine the success of the biosensor construction process. Figure 4a shows the curve of the photocurrent during the modification process, bare ITO electrode displayed a nearly zero PEC response (curve a), and after defective TiO_{2-x} dropped onto the ITO electrode, an obvious photocurrent was observed (curve b). Then, MB-Ab_1 bioconjugate was decorated on the electrode, due to the excellent photosensitivity of dye; an enhanced photocurrent was achieved (curve c); and the increased PEC response demonstrated that these two photoactive materials were successfully modified on the electrode. Next, BSA (curve d) was modified on the photosensitive surface to block the non-specific active sites, following Ag (curve e), liposome@L-Cysteine-Ab_2 (curve f) were then dropped on the electrode, and the photocurrent displayed a reduced trend due to the non-conductivity of these biomolecules (the above PEC measurements were performed in a pristine PBS buffer solution). When a suitable amount of tween was added in the PBS solution, the liposome was resolved, and the L-Cysteine (electron donor) released and reacted with photo-generated holes, thus increasing the photocurrent (curve g). The obtained results indicate that the PEC immunosensor was successfully developed.

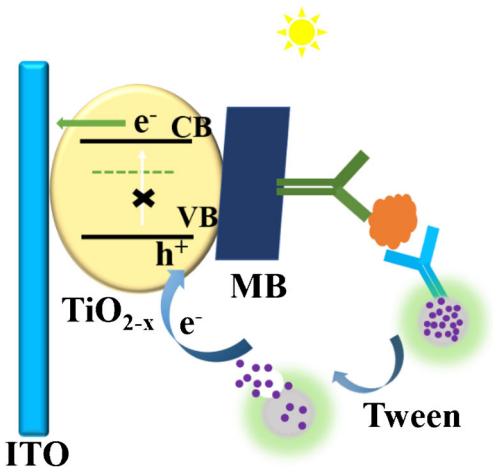

Fig. 3 The possible electron transfer mechanism of the developed biosensor

Electrochemical impedance spectroscopy (EIS) is another characterization means to photocurrent for efficient evaluating whether the PEC biosensor construction triumphantly. As shown in Fig. 4b, bare ITO displayed a small impedance value (curve a); after TiO_{2-x} (semi-conductor) dropped, an enhanced resistance value (curve b) was obtained. After that, the MB-Ab_1 was modified, and a bigger resistance value (curve c) was achieved. Then, the non-conductive biomolecules of BSA

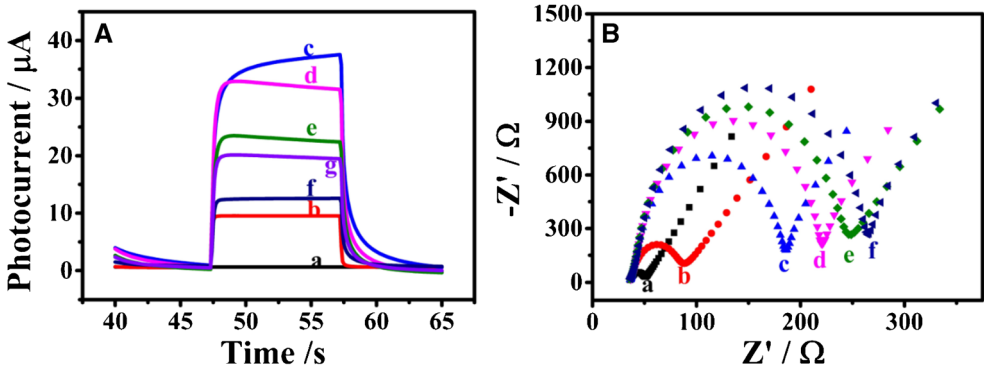

Fig. 4 The (A) photocurrent curve and (B) EIS curve during the layer-by-layer construction processes. (a) bare ITO, (b) ITO/TiO_{2-x}, (c) ITO/TiO_{2-x}/MB-Ab_1, (d) ITO/TiO_{2-x}/MB-Ab_1/BSA, (e) ITO/TiO_{2-x}/MB-Ab_1/BSA/Ag, (f) ITO/TiO_{2-x}/MB-Ab_1/BSA/Ag/liposome@L-Cysteine-Ab_2 (PBS solution), (g) ITO/TiO_{2-x}/MB-Ab_1/BSA/Ag/liposome@L-Cysteine-Ab_2 (PBS solution with tween). (c_{Ag} = 0.1 ng/mL)

(curve d), Ag (curve e), and Ab_2-liposome@L-Cysteine (curve f) were decorated on the electrode via the layer-by-layer process, and the resistance was gradually increased, which further prove the resounding fabrication of the PEC biosensor.

Analytical performance of CYFRA 21-1

Under the preferred measurement conditions (the test results are shown in Fig. S3), a signal-on biosensor with the PEC detection was performed for CYFRA 21-1 supported by the controlled electron donor release strategy. When the low concentration of Ag was modified, the fixed liposome@L-Cysteine-Ab_2 was less; hence, the less L-Cysteine was released, and a smaller change in photocurrent was obtained. As the concentration of Ag gradually increased, the change in photocurrent was gradually increased (Fig. 5a). As can be seen from Fig. 5b, the developed PEC biosensor has a linear photocurrent signal in the range of 0.0001–100 ng/mL, the calibration equation is given by $I = 23.32 + 2.396\log c$(ng/mL) ($R^2 = 0.9986$), and the detection limit was as low as 0.037 pg/mL ($S/N = 3$). The developed PEC biosensor is compared with other relevant methods for the CYFRA 21-1 detection which are displayed in Table S2 in ESM file.

To analyze the target more accurately, the stability and reproducibility of the constructed PEC biosensor were considered. In this item, the stability of the biosensor was determined via continuous photocurrent detection of the electrodes for 15 cycles, and acceptable stability was obtained (Fig. 5c). The storage lifetime was also analyzed to characterize the storage stability of the sensor, and the results are shown in Fig. S5. As can be seen, in the first week of the sensor storage,

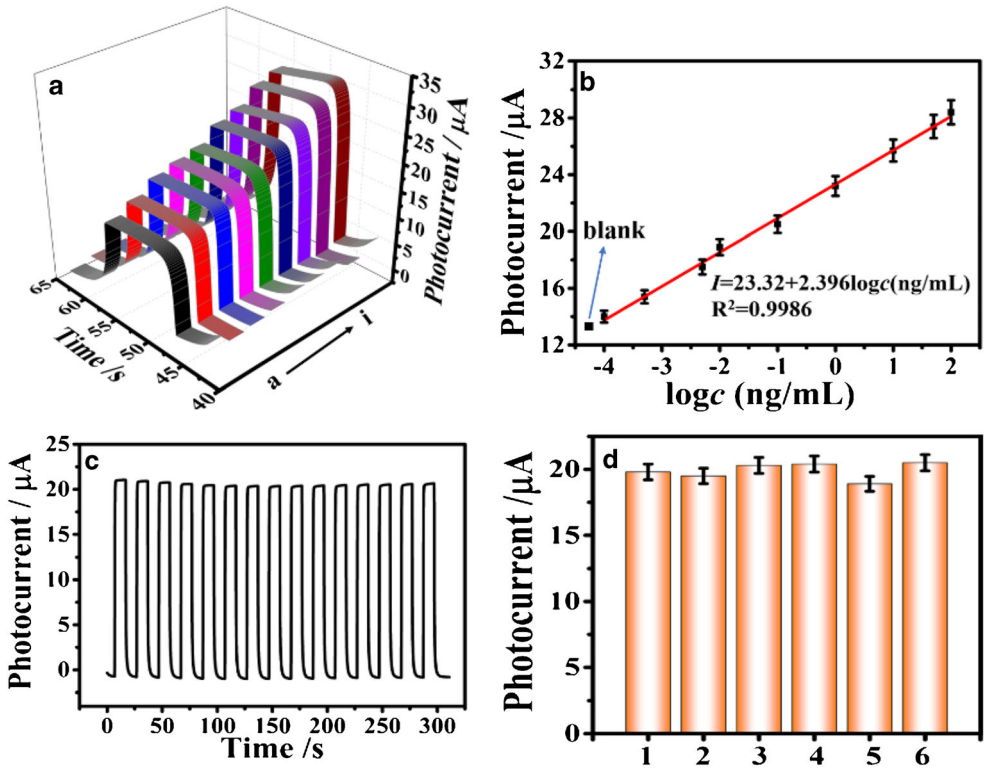

Fig. 5 The property analysis of the CYFRA 21-1. (A) PEC calibration curve of different concentrations and (B) linear relationship of the biosensor: (a–i) 0.0001, 0.0005, 0.005, 0.01, 0.1, 1, 10, 50, 100 ng/mL. (C) Stability analysis and (D) reproducibility analysis. (c_{Ag} = 0.1 ng/mL). Error bars = SD (n = 3)

the signal was reduced to 97% of the original response, and after another week, the signal was reduced to 92% of the original response, which means the sensor can still reach considerable detection standards after 2 weeks of storage. To analyze reproducibility, six electrodes prepared under the same conditions were tested, and the results are shown in Fig. 5d; the relative standard deviation (RSD) value (3.13%) illustrates the excellent reproducibility of the PEC biosensor. As another important consideration for PEC sensor, the selectivity was analyzed, and the result is depicted in Fig. S5 in ESM file. The RSD were 2.73 and 3.57% which confirm that the biosensor also exhibited a great selectivity.

Real sample analysis

The significance of the successful construction of biosensor lies in the accuracy detection of real sample. The results of five parallel experiments are shown in Table S3. The recovery rate was between 97.4 and 101.4% and 98.3 and 104.4%. The RSD are both below 5%, which demonstrates the potential application value in the clinical detection of CYFRA 21-1. However, it implies that the sensor has certain limitations in analyzing complex samples, and requires complex pretreatment prior to analysis.

Conclusion

A novel signal-on PEC biosensor was successfully developed via a skillful electron donor controlled-release system. The organic dye methylene blue-sensitized defective TiO_{2-x} provided a large and stable basic photoelectrochemical signal for biosensor construction. And L-cysteine as electron donor was encapsulated in liposomes to enhance the stability and sensitivity of the sensor. Such developed PEC biosensor provides a reference method for detecting other cancer markers or other small biomolecules, and the signal amplification strategy also provides an application basis for other electrochemical methods. Although this skillful signal amplification strategy provides a great PEC performance for target detection, the accurate detection of real samples is still a challenge for future studies.

Supplementary Information The online version contains supplementary material available at https://doi.org/10.1007/s00604-021-04721-4.

Funding This study was supported by the National Key Scientific Instrument and Equipment Development Project of China (No. 21627809), National Natural Science Foundation of China (Nos. 21777056), Special Foundation for Taishan Scholar Professorship of Shandong Province, Jinan Scientific Research Leader Workshop Project (2018GXRC024, 2018GXRC021), and the Innovation Team Project of Colleges and Universities in Jinan (No.2019GXRC027).

Declarations

Conflict of interest The authors declare that they have no known competing financial interests or personal relationships that could have appeared to influence the work reported in this paper.

References

1. Smeltzer MP, Wynes MW, Lantuejoul S, Soo R, Ramalingam SS, Varella-Garcia M, Meadows Taylor M, Richeimer K, Wood K, Howell KE, Dalurzo ML, Felip E, Hollenbeck G, Kerr K, Kim ES, Mathias C, Pacheco J, Postmus P, Powell C, Tsuboi M, Wistuba II, Wakelee HA, Belani CP, Scagliotti GV, Hirsch FR (2020) The international association for the study of lung cancer (IASLC) global survey on molecular testing in lung cancer. J thoracic oncol 15:1434–1448. https://doi.org/10.1016/j.jtho.2020.05.002
2. Garcia E, Picciotto S, Neophytou AM, Bradshaw PT, Balmes JR, Eisen EA (2018) Lung cancer mortality and exposure to synthetic metalworking fluid and biocides: controlling for the healthy worker survivor effect. Occup Environ Med 75:730–735
3. Fu L, Wang R, Yin L, Shang XP, Zhang RT, Zhang PJ (2019) CYFRA21-1 tests in the diagnosis of non-small cell lung cancer: a meta-analysis. Int J Biol Markers 34:251–261
4. Wang JB, Jiang W, Zhang T, Liu LP, Bi N, Wang XZ et al (2018) Increased CYFRA 21-1, CEA and NSE are prognostic of poor outcome for locally advanced squamous cell carcinoma in lung: a nomogram and recursive partitioning risk stratification analysis. Transl Oncol 11:999–1006
5. Lai RS, Hsu HK, Lu JY, Ger LP, Lai NS (1996) CYFRA 21-1 enzyme-linked immunosorbent assay. Evaluation as a tumor marker in non-small cell lung cancer. Chest 109:995–1000
6. Liu S, Jia Y, Xue J, Li Y, Wu Z, Ren X, Ma H, Li Y, Wei Q (2020) Bifunctional peptide-biomineralized gold nanoclusters as electrochemiluminescence probe for optimizing sensing interface. Sens Actuators B-Chem 318:128278
7. S. Kumar, S. Kumar, S. Tiwari, S. Augustine, S. Srivastava, B.K. Yadav, et al. (2016) Highly sensitive protein functionalized nanostructured hafnium oxide based biosensing platform for non-invasive oral cancer detection. Sens. Actuators, B-Chemi 235:1-10
8. He A, Liu TC, Dong ZN, Ren ZQ, Hou JY, Li M, Wu YS (2013) A novel immunoassay for the quantization of CYFRA 21-1 in human serum. J Clin Lab Anal 27:277–283
9. Hou T, Xu N, Wang W, Ge L, Li F (2018) Truly immobilization-free diffusivity-mediated photoelectrochemical biosensing strategy for facile and highly sensitive microRNA assay. Anal Chem 90: 9591–9597
10. Li H, Wang J, Wang X, Lin H, Li F (2019) Perylene-based photoactive material as a double-stranded DNA intercalating probe for ultrasensitive photoelectrochemical biosensing. ACS Appl Mater Interfaces 11:16958–16964
11. Song X, Hou T, Lu F, Wang Y, Liu J, Li F (2020) Homogeneous photoelectrochemical biosensing via synergy of G-quadruplex/hemin catalysed reactions and the inner filter effect. Chem Commun 56:1811–1814
12. Li HB, Li J, Zhu YY, Xie WY, Shao R, Yao XX et al (2018) Cd^{2+}-doped amorphous TiO_2 hollow spheres for robust and ultrasensitive photoelectrochemical sensing of hydrogen sulfide. Anal Chem 90: 5496–9502
13. Tian JY, Li Y, Dong JJ, Huang MJ, Lu JS (2018) Photoelectrochemical TiO_2 nanotube arrays biosensor for asulam

determination based on in-situ generation of quantum dots. Biosens Bioelectron 110:1–7
14. Lima F, Freires ADS, Pereira NDM, Silva GG, da Rocha CQ, Damos FS et al (2018) Photoelectrochemical sensing of tannic acid based on the use of TiO_2 sensitized with 5-methylphenazinium methosulfate and carboxy-functionalized CdTe quantum dots. Mikrochim Acta 185:521
15. Shu J, Qiu Z, Lv S, Zhang K, Tang D (2018) Plasmonic enhancement coupling with defect-engineered TiO_{2-x}: a mode for sensitive photoelectrochemical biosensing. Anal Chem 90:2425–2429
16. Zhang H, Tao T, Li X, Bao Y, Xia X, Lourenço M, Homewood K, Huang Z, Gao Y (2020) Extending the detection range and response of TiO_2 based hydrogen sensors by surface defect engineering. Inter. J. Hydrogen Energy 45:18057–18065
17. Bahmanrokh G, Cazorla C, Mofarah SS, Shahmiri R, Yao Y, Ismail I, Chen WF, Koshy P, Sorrell CC (2020) Band gap engineering of Ce-doped anatase TiO_2 through solid solubility mechanisms and new defect equilibria formalism. Nanoscale 12:4916–4934
18. Feng S, Wang T, Liu B, Hu C, Li L, Zhao ZJ, Gong J (2020) Enriched surface oxygen vacancies of photoanodes by photoetching with enhanced charge separation. Angew Chem Int Ed Engl 59:2044–2048
19. Liu Y, Li J, Tang H, Li W, Yang Y, Li Y, Chen Q (2016) Enhanced photoelectrochemical performance of plate-like WO_3 induced by surface oxygen vacancies. Electrochem Commun 68:81–85
20. Pan X, Chen X, Yi Z, Defective (2016) Porous TiO_2 nanosheets with Pt decoration as an efficient photocatalyst for ethylene oxidation synthesized by a C_3N_4 templating method. ACS Appl Mater Interfaces 8:10104–10108
21. Ning DD, Wei HH, Ou G, Zhang RY, Wu H (2018) Copper reduced defective TiO_2 nanoparticles with enhanced visible light photocatalytic activity. J Am Ceram Soc 101:4857–4863
22. Ning X, Lu B, Zhang Z, Du P, Ren H, Shan D et al (2019) An efficient strategy for boosting photogenerated charge separation by using porphyrins as interfacial charge mediators. Angew Chem Int Ed Engl 58:16800–16805
23. Song K, Ding C, Zhang B, Chang H, Zhao Z, Wei W, Wang J (2018) Dye sensitized photoelectrochemical immunosensor for the tumor marker CEA by using a flower-like 3D architecture prepared from graphene oxide and MoS_2. Mikrochim Acta 185:310
24. Li MJ, Wang HJ, Yuan R, Chai YQ (2019) A zirconium-based metal-organic framework sensitized by thioflavin-T for sensitive photoelectrochemical detection of C-reactive protein. Chem Commun 55:10772–10775
25. Tsui L-k, Huang J, Sabat M, Zangari G (2014) Visible light sensitization of TiO_2 nanotubes by bacteriochlorophyll-C dyes for photoelectrochemical solar cells. ACS Sustain Chem Eng 2:2097–2101
26. Xu R, Liu L, Liu X, Li Y, Feng R, Wang H, Fan D, Wu D, Wei Q (2020) Novel electron donor encapsulation assay based on the split-type photoelectrochemical interface. ACS Appl Mater Interfaces 12:7366–7371
27. Kamaly N, Yameen B, Wu J, Farokhzad OC (2016) Degradable controlled-release polymers and polymeric nanoparticles: mechanisms of controlling drug release. Chem Rev 116:2602–2663
28. Zhou Q, Lin Y, Lu M, Tang D (2017) Bismuth ferrite-based photoactive materials for the photoelectrochemical detection of disease biomarkers coupled with multifunctional mesoporous silica nanoparticles. J Mater Chem B 5:9600–9607
29. Mei LP, Liu F, Pan JB, Zhao WW, Xu JJ, Chen HY (2017) Enediol-ligands-encapsulated liposomes enables sensitive immunoassay: a proof-of-concept for general liposomes-based photoelectrochemical bioanalysis. Anal Chem 89:6300–6304
30. Xue TY, Mei LP, Xu YT, Liu YL, Fan GC, Li HY, Ye D, Zhao WW (2019) Nanoporous semiconductor electrode captures the quantum dots: toward ultrasensitive signal-on liposomal photoelectrochemical immunoassay. Anal Chem 91:3795–3799
31. Huang L, Yang L, Zhu C, Deng H, Liu G, Yuan Y (2018) Methylene blue sensitized photoelectrochemical biosensor with 3,4,9,10-Perylene tetracarboxylic acid film as photoelectric material for highly sensitive Pb^{2+} detection. Sens Actuators, B-Chem 274:458–463